Nanocrystalline CePO$_4$:Tb as a novel oxygen sensing material on the basis of its redox responsive reversible luminescence

Nanocrystalline CePO$_4$:Tb as a novel oxygen sensing material on the basis of its redox responsive reversible luminescence

Weihua Di[1], Xiaojun Wang and Xinguang Ren

Key Laboratory of Excited State Processes, Changchun Institute of Optics, Fine Mechanics and Physics, Chinese Academy of Sciences, Changchun, 130033, People's Republic of China

E-mail: weihdi@yahoo.com.cn

Abstract
This work reports for the first time on a new finding of luminescent CePO$_4$:Tb nanocrystals providing a novel oxygen sensing material on the basis of the redox responsive reversible luminescence in an oxidizing/reducing atmosphere. The origin of the luminescence quenching/recovery of nanocrystalline CePO$_4$:Tb was clearly demonstrated, from the surface chemistry of nanocrystals and the fluorescence decay dynamics of Tb(III). Our present work represents a preliminary demonstration of the feasibility of using nanocrystalline CePO$_4$:Tb as a novel oxygen sensing material since it yields several advantages including surfactant-free synthesis, dual detection functioning, rapid response, high sensitivity and good reproducibility.

S Supplementary data are available from stacks.iop.org/Nano/21/075709/mmedia

(Some figures in this article are in colour only in the electronic version)

1. Introduction

Rapid progress in the synthesis and fundamental understanding of surface phenomena have generated great excitement as regards incorporation of nanomaterials into sensor architectures [1]. Nanomaterials are strong candidates for analyte detection use, because the reduced size leads to an exceptionally high surface area and creates a remarkable increase in the sensor sensitivity towards changes in the chemical environment [2].

The successful applications of rare-earth-based luminescent bulk materials as phosphors used in lighting and displays have inspired great research interest in their nanoscale counterparts [3]. For luminescent nanoscaled rare-earth compounds, the decreased size presents particular photophysical properties, different from those observed from the bulk materials, and finds novel potential for use in optoelectronic nanodevices and biological fluorescence labeling [4].

In the rare-earth element, there are several redox couples, such as Eu(II)/Eu(III), Yb(II)/Yb(III), and Ce(III)/Ce(IV). The valence variation of rare-earth cations can lead to a significant difference in photoluminescence properties.

Ce(III)PO$_4$:Tb(III) is an excellent green emitter due to a strong absorption of Ce(III) within the UV range followed by an efficient energy transfer from Ce(III) to Tb(III), leading to a strong emission of Tb(III) [5]. Unfortunately, Ce(III) is oxidized easily in the oxidizing environment, thus resulting in the formation of Ce(IV), which quenches the luminescence of Tb(III) significantly [6].

Interestingly, on the basis of significant luminescence quenching due to Ce(III) oxidation, we find a new application of nanocrystalline CePO$_4$:Tb as a novel oxygen sensing material. The luminescence quenching of CePO$_4$:Tb becomes a useful probe for the recognition and detection of oxygen molecules. Herein, we are for the first time reporting the potential of luminescent nanocrystalline CePO$_4$:Tb as a novel oxygen sensor on the basis of its redox responsive luminescence in oxidizing/reducing atmosphere.

2. Experimental details

2.1. Synthesis of materials

Nanocrystalline CePO$_4$:Tb was synthesized by a simple aqueous route based on the standard Schlenk technique.

---

[1] Author to whom any correspondence should be addressed.

Typically, 1.8 mmol $CeCl_3$ and 0.2 mmol of $TbCl_3$ were dissolved in 60 ml of distilled water to make a clear solution in a vessel. The vessel was subjected to a vacuum to remove gases, and then refilled with inert gas by using the standard Schlenk line technique. Subsequently, the solution was injected into a three-necked flask under an Ar atmosphere, and heated to 80 °C. 3 mmol of H_3PO_4 dispersed in the distilled water under an Ar atmosphere was injected into the above solution. The resulting mixture was kept at 80 °C with magnetic stirring for 5 h. The resulting precipitates were centrifugally separated, and washed several times with distilled water, and then dried in vacuum at 40 °C overnight. The as-synthesized product is a hydrated compound since an endothermic peak around 220 °C in the DTA curve is observed due to the presence of structural water (figure S1 in the supporting information (SI), available at stacks.iop.org/Nano/21/075709/mmedia). The as-synthesized product was annealed at 300 °C in a reducing atmosphere for 2 h to remove structural water.

2.2. Characterization

The x-ray powder diffraction (XRD) data were collected using an X'Pert MPD Philips diffractometer (Cu Kα x-radiation at 40 kV and 50 mA). Scanning electron microscopy (SEM) images were recorded using a FEG-SEM Hitachi SU-70 microscope operating at 4 kV at a working distance of 2–3 mm. For the SEM observations, samples were prepared without any carbon coating simply by depositing some powder onto a double gluing tape. High resolution transmission electron microscopy (HRTEM) investigations were carried using a JEOL 2200FS microscope. Samples for TEM investigations were prepared by first dispersing the particles in ethanol with the assistance of ultrasonication and then dropping one drop of the suspension onto a copper TEM grid coated with a holey carbon film.

XPS analysis was performed using a PHI Quantera SXM (ULVAC-PHI) device operating at a pressure of 10^{-8} Torr. The photoelectron emission spectra were recorded using a monochromatic Al Kα source (100 W). The angle between the x-ray direction and the emitted electron direction was 45°.

The emission of $CePO_4$:Tb nanocrystals was measured using a Hitachi-4500 fluorescence spectrophotometer equipped with a xenon lamp (150 W) operating in the 200–900 nm range. The emission spectra of different samples were obtained upon excitation into the Ce^{3+} 4f–5d absorption, and the excitation spectra were monitored at the emission of the Tb^{3+} $^5D_4$–$^7F_5$ transition.

The excited state lifetimes of samples were measured using a conventional Nd:YAG (neodymium yttrium aluminum garnet) laser system (Spectra Physics). The linewidth, repetition frequency, and pulse duration of the laser light were 1 cm^{-1}, 10 Hz, and 10 ns. The excitation source was the 266 nm output from the Nd:YAG laser combined with a fourth-harmonic generator. The fluorescence decay of Tb^{3+} $^5D_4$ for the samples exposed to an atmosphere containing oxygen was fitted with a double-exponential function: $y = A_1^* \exp(-x/\tau_1) + A_2^* \exp(-x/\tau_2)$. The average lifetime was obtained by $\langle \tau \rangle = (A_1^2 \tau_1^2 + A_2^2 \tau_2^2)/(A_1 \tau_1 + A_2 \tau_2)$.

The absolute emission quantum yield was measured at room temperature using a quantum yield measurement system C9920-02 from Hamamatsu with a 150 W xenon lamp coupled to a monochromator for wavelength discrimination, an integrating sphere as the sample chamber and a multi-channel analyzer for signal detection. Three measurements were made for each sample and the average value is reported.

3. Results and discussion

The product corresponds to hexagonal rhabdophane-type $CePO_4$ crystals, as revealed by x-ray diffraction studies (JCPDS No. 34-1380; figure S2 in SI, available at stacks.iop.org/Nano/21/075709/mmedia). A scanning electron microscopy image (figure 1(a)) reveals the rod-like morphology of products. High resolution transmission electron microscopy (TEM) studies provide deep insight into the crystalline size and quality, and preferential growth axis (figures 1(b) and (c)). The products are single-crystalline nanorods with the width of 10–20 nm. They are perfectly crystallized without visible defects and dislocations, revealing high crystalline quality. The calculated interplanar distance is about 0.64 nm, corresponding to the separation of the (001) crystal plane. This indicates that the growth of the particles along the c-axis $\langle 001 \rangle$ is favored, leading to the observed rod-shaped particles with high aspect ratio.

The photoluminescence of $CePO_4$:Tb is based on an efficient energy transfer from Ce(III) to Tb(III) (figure S3 in SI, available at stacks.iop.org/Nano/21/075709/mmedia). Nanocrystalline $Ce_{0.9}PO_4$:$Tb_{0.1}$ synthesized in our work shows a high luminescence quantum yield of 50% for Tb(III) emission. If Ce(III) emission is included, the quantum yield is as high as 65%.

Nanocrystalline $CePO_4$:Tb presents a significant and rapid decrease of luminescence upon exposure to an oxygen atmosphere at 200 °C, as observed in figure S4 (see the supporting information, available at stacks.iop.org/Nano/21/075709/mmedia). The luminescence decreases rapidly to 15% in the first a few minutes, and this is followed by a slow decrease in subsequent time. Compared to nanocrystalline $CePO_4$:Tb, bulk $CePO_4$:Tb (1–3 μm in size) prepared by solid state reaction shows a negligible decrease of luminescence (∼5%). This comparison clearly shows a noticeable size effect on the luminescence quenching of $CePO_4$:Tb upon exposure to the oxygen atmosphere. The reduction of the size of $CePO_4$:Tb particles results in a markedly enhanced response to changes in the surrounding environment. The noticeable luminescence quenching of nanocrystalline Ce(III)-containing emitters was observed by other groups. The Boilot group has reported the luminescence decrease of nanocrystalline $LaCe_{0.45}Tb_{0.15}PO_4$ by 95% when it is exposed to air at 200 °C [7]. Most of the related research has been devoted to improving the thermal stability against oxygen and the luminescence quantum yield of $CePO_4$:Tb nanocrystals, but neglected its usefulness in luminescence quenching that might enable its new application in other technological areas. In particular, our work surprisingly finds that the luminescence can be recovered to the initial level when nanocrystalline
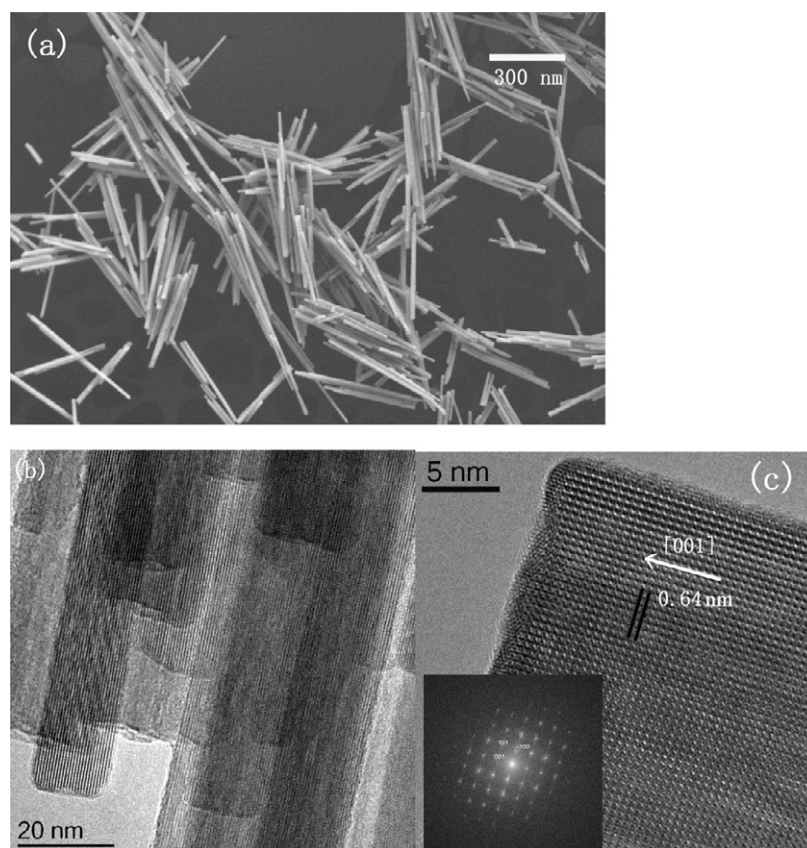
Figure 1. Typical SEM (a) and HRTEM ((b) and (c)) images of CePO$_4$:Tb.

CePO$_4$:Tb if it has ever been subjected to O$_2$ was exposed to a reducing atmosphere (95% N$_2$/5% H$_2$) at a slightly higher temperature, 250 °C, for several minutes (figure S4 in SI, available at stacks.iop.org/Nano/21/075709/mmedia). The significant luminescence quenching and reversible luminescence effect demonstrate the capabilities of nanocrystalline CePO$_4$:Tb as a sensing material.

The mechanism of luminescence quenching of nanocrystalline CePO$_4$:Tb in the presence of oxygen has not been understood well up to now. To clarify the origins of the fluorescence quenching and recovery in the presence/absence of O$_2$, respectively, x-ray photoelectron spectroscopy (XPS) was used to determine the local atomic environment and chemical states of the material surface. Figure 2 presents the Ce 3d XPS spectra of the original CePO$_4$:Tb nanocrystals and those samples exposed to different atmospheres. For the original sample, the Ce $3d_{3/2,5/2}$ spectra are composed of two multiplets (v and u) corresponding to the spin–orbit split $3d_{5/2}$ and $3d_{3/2}$ core holes, respectively. The four peaks resolved from this pair of spin–orbit doublets can be identified as those of the Ce(III) state: the higher binding energy peaks, u' and v', located at about 903.8 ± 0.1 eV and 885.4 ± 0.1 eV, respectively, result from the Ce $3d^9 4f^1 O\ 2p^6$ final state, while the lower binding energy ones, u'' and v'', located at 900.8 ± 0.1 eV and 882 ± 0.1 eV, result from Ce $3d^9 4f^2 O\ 2p^5$ [8]. However, for the samples exposed to O$_2$ at 200 °C, an additional peak located at 917 eV is clearly observed. This peak is characteristic of the Ce(IV) state originating from the Ce $3d^9 4f^0 O\ 2p^6$ final state [8]. This clearly demonstrates
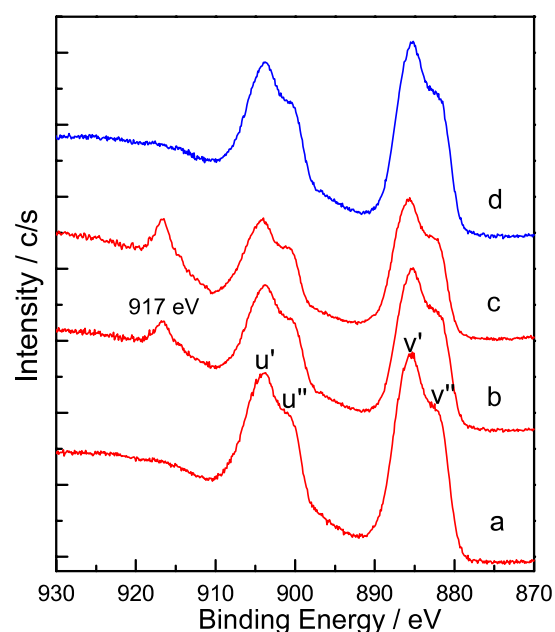

Figure 2. X-ray photoelectron spectra recorded from Ce $3d_{3/2,5/2}$. Original CePO$_4$:Tb (a); exposed to 50% O$_2$/50% N$_2$ (b) and 100% O$_2$ (c), respectively, at 200 °C for 5 min; exposed first to 100% O$_2$ at 200 °C for 5 min and then to a reducing atmosphere at 250 °C for 10 min (d).

the presence of Ce(IV) at the surface for samples exposed to O$_2$. The peak intensity of the Ce(IV) state increases, whereas the peak intensity of the Ce(III) state decreases as the O$_2$
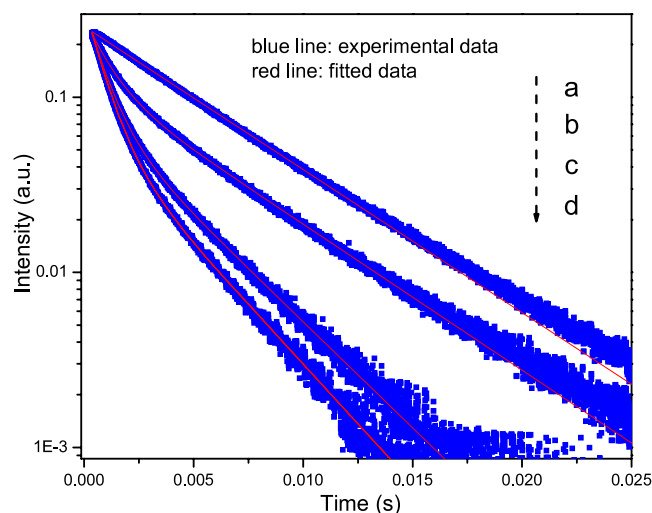
Figure 3. Fluorescent decay of $^5D_4$ of Tb(III) for nanocrystalline CePO$_4$:Tb. Original sample (a) and those exposed to 40% (b), 80% (c) and 100% (d) oxygen atmospheres at 200 °C for 5 min, respectively. Curve a was fitted with a mono-exponential function, while curves (b), (c), and (d) were fitted with a bi-exponential function.

Figure 4. Plots of fluorescence quenching (a) and lifetime (b) versus oxygen concentration. Here, I_0/I and τ_0/τ were used to indicate the influence of O$_2$ on the emission intensity and excited state lifetime of Tb^{3+}. I_0 and τ_0 denote the emission intensity and excited state lifetime in the absence of O$_2$; I and τ denote the presence of O$_2$.

concentration increases. When the sample subjected to thermal oxidation was exposed to a reducing atmosphere N$_2$/H$_2$ for several minutes, the signal indicative of Ce(IV) located at 917 eV totally disappeared, and the initial Ce(III) state was fully recovered (curve d in figure 2). This demonstrates the reduction of the oxidized states of nanocrystalline CePO$_4$. However, no change was observed for Tb 4d XPS spectra of the samples before and after exposure to oxygen (figure S5 in SI, available at stacks.iop.org/Nano/21/075709/mmedia). The above results show that Ce(III) in the oxygen atmosphere can be oxidized to Ce(IV), which can reversibly return to Ce(III) in the reducing atmosphere—that is, a reversible transition of Ce(III) → Ce(IV) → Ce(III).

Obviously, the presence of Ce(IV) at the expense of Ce(III) reduces the energy transfer from Ce(III) to Tb(III) significantly, thus leading to the luminescence quenching of nanocrystalline CePO$_4$:Tb. Here, we find another important reason for the luminescence quenching in the presence of Ce(IV) by measuring the fluorescent decay for the original sample and those exposed to different concentrations of O$_2$ (figure 3). The original sample shows an almost mono-exponential luminescence decay with a long excited state lifetime, whereas the decay for samples subjected to thermal oxidation strongly deviates from mono-exponential decay behavior, showing a fast decay component and a slow component. The fast decay component should originate from the fluorescent decay of Tb(III) in proximity to Ce(IV) through a nonradiative energy transfer from the excited state of Tb(III) to Ce(IV). When the O$_2$ concentration increases, the fast decay becomes more pronounced due to the increase of the amount of Ce(IV) state. However, the fluorescence decay can be reversibly recovered to the initial level (not shown) due to a reversible transition of Ce(IV) → Ce(III) when the sample is reduced in an N$_2$/H$_2$ atmosphere at 250 °C for
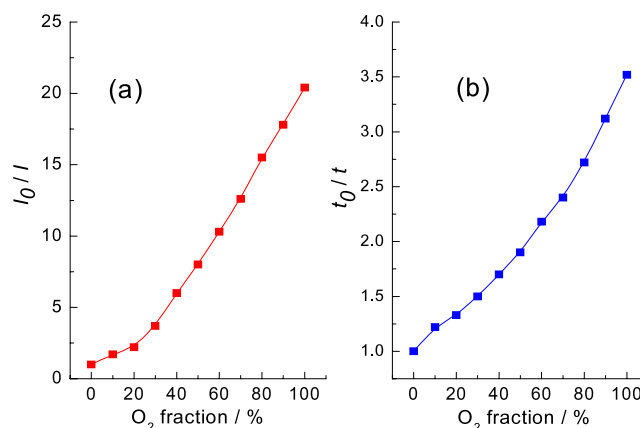
several minutes. This fully demonstrates that Ce(IV) actually acts as nonradiative transition channels that speed up the luminescence decay of the excited state of Tb^{3+}, leading to decrease of the emission intensity and excited state lifetime of Tb(III). As regards the luminescence quenching mechanism, Ce(IV), therefore, plays a double role. On the one hand, the presence of Ce(IV) obviously breaks the energy transfer from Ce(III) to Tb(III); on the other hand, it creates the nonradiative radiation paths through the energy transfer from the excited state of Tb(III) to Ce(IV). The reversible transition of Ce(III) → Ce(IV) → Ce(III) is the origin of the luminescence quenching and recovery.

Stern–Volmer plots shown in figure 4 present the oxygen sensing properties of nanocrystalline CePO$_4$:Tb in terms of the photoluminescence (I) and excited state lifetime (τ) of Tb(III). The luminescence quenching increases from 36% to 96% as the concentration of the oxygen atmosphere varies from 10% to 100% and, simultaneously, the fluorescence lifetime of the $^5D_4$ state of Tb^{3+} decreases from 3.56 to 0.98 ms. Indeed, monitoring oxygen through τ is advantageous over monitoring I, since τ is independent of the variation in the intensity of the excitation source [9]. Furthermore, Tb(III) ions commonly show a relatively long excited state lifetime (~ms), which can ensure the sensitivity and accuracy of the detection. Therefore, either change of I or change of τ for Tb(III) can be used as a probe to monitor the oxygen molecules for our present CePO$_4$:Tb sensing system. This further demonstrates the fascinating potential of nanocrystalline CePO$_4$:Tb as a gas sensing material. It can be seen that both $I_0/I \sim$ O$_2$ % (figure 4(a)) and $\tau_0/\tau \sim$ O$_2$% (figure 4(b)) plots give nonlinear relationships. The heterogeneous distribution of Ce(IV) may be responsible for the nonlinear Stern–Volmer plots. As we know, Ce(IV) ions are mostly distributed at the surface of particles, because it is difficult for oxygen to diffuse into the interior of particles in a short time. Therefore, Tb(III) ions are located in two different local environments: distributed on the surface of particles where Tb(III) ions are very close to Ce(IV) and in the interior of particles where
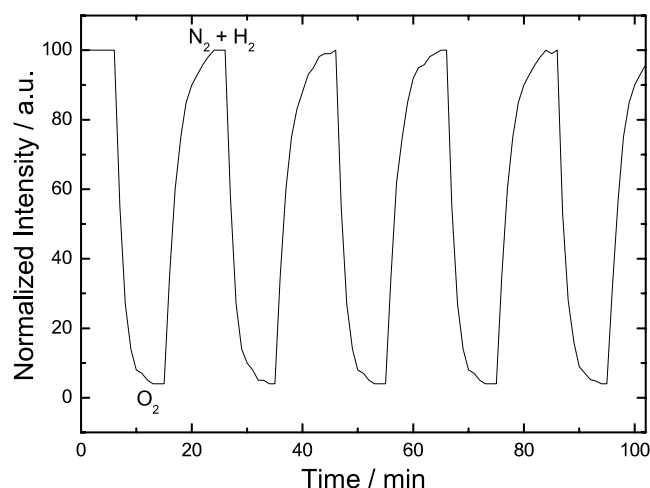
Figure 5. Emission intensity of nanocrystalline CePO$_4$:Tb as a function of time when subjected to an atmosphere which was varied periodically between 100% O$_2$ and 95% N$_2$/5%H$_2$.

Tb(III) ions are relatively far from Ce(IV). Obviously, the luminescence of Tb(III) close to the surface is more heavily quenched than that of Tb(III) located in the interior. As a result, the different degrees of luminescence quenching of Tb(III) distributed in two local different environments result in nonlinear Stern–Volmer curves [10]. It is also observed from Stern–Volmer plots that oxygen sensing CePO$_4$:Tb shows a high sensing sensitivity. Even at a low O$_2$ concentration of 10%, the luminescence quenching reaches 36%. This indicates that CePO$_4$:Tb nanocrystals have the potential to detect low contents of O$_2$ in certain specific environments. The detection sensitivity is well known to relate to the particle size of sensing materials. CePO$_4$:Tb nanorods synthesized in our work have a relatively large surface-to-volume ratio with a specific surface area of 176 m^2 g^{-1}. This effectively enhances the interaction between the exposed surface of the sensing materials and analyte molecules, and leads to a relatively high detection sensitivity [11]. In addition, the high luminescence quantum yield also contributes greatly to the sensitivity of sensing materials since a high value of I_0/I can be readily obtained [9]. Since parameters such as size, morphology, and photoluminescence quantum yield are able to influence the sensing properties, further research is under way on controlling the size, morphology and crystallinity and optimizing the photoluminescence efficiency of the nanocrystals. We expect these works to further reveal the correlation of sensing properties (e.g. sensitivity, response time) with these parameters.

For gas sensing materials, the response and recovery time and the reproducibility are very important in practical applications. Figure 5 shows the response and recovery characteristics of sensing CePO$_4$:Tb nanorods upon exposure to an alternating atmosphere of 100% O$_2$ and 95% N$_2$/5% H$_2$. A fast response of luminescence quenching and recovery was clearly observed. After performing several oxidation/reduction cycles, a reproducible signal can still be obtained, indicating high stability of the CePO$_4$:Tb sensing materials.

4. Conclusion

In summary, we observed for the first time the reversible luminescence response of nanocrystalline CePO$_4$:Tb under an oxidizing/reducing atmosphere, which can potentially be used as a novel gas sensing material. XPS and fluorescence decay reveal the exact origin of the luminescence quenching/recovery of CePO$_4$:Tb. Overall, our present work represents a preliminary demonstration of the feasibility of using nanocrystalline CePO$_4$:Tb as a novel gas sensing material since it shows several advantages, such as simple surfactant-free fabrication, dual detection functioning via the luminescence intensity and lifetime, high sensitivity, high photostability and good reproducibility.

Acknowledgments

References

[1] Franke M, Koplin T and Simon U 2006 *Small* **2** 36
    Kauffman D and Star A 2008 *Angew. Chem. Int. Edn* **47** 6550
    Zhu Y F, Lian J S and Jiang Q 2009 *J. Phys. Chem.* C **113** 16896
[2] Banthia S and Samanta A 2006 *J. Phys. Chem.* B **110** 6437
    Zhu Y, Lang X and Jiang Q 2008 *Adv. Funct. Mater.* **18** 1422
    Pinna N, Neri G, Antonietti M and Niederberger M 2004 *Angew. Chem. Int. Edn* **43** 4345
[3] Di W H, Wang X J, Chen B J, Lai H S and Zhao X X 2005 *Opt. Mater.* **27** 1386
    Luo Q, Shen S, Lu G, Xiao X, Mao D and Wang Y 2009 *J. Mater. Chem.* **19** 8079
    Su Y, Li L and Li G 2008 *Cryst. Growth Des.* **8** 2678
    Li L, Sun H, Fang C, Xu J, Jin J and Yan C 2007 *J. Mater. Chem.* **17** 4492
    Pan G, Song H, Bai X, Liu Z, Yu H, Di W, Li S, Fan L, Ren X and Lu S 2006 *Chem. Mater.* **18** 4526
[4] Wong K, Law G, Murphy M, Tanner P, Wong W, Lam P and Lam M 2008 *Inorg. Chem.* **47** 5190
    Yan Z and Yan C 2008 *J. Mater. Chem.* **18** 5046
    Di W, Willinger M, Ferreira R, Ren X, Lu S and Pinna N 2008 *J. Phys. Chem.* C **112** 18815
[5] Zhu H, Zhu E, Yang H, Wang L, Jin D and Yao K 2008 *J. Am. Ceram. Soc.* **91** 1682
[6] Riwotzki K, Meyssamy H, Kornowski A and Hasse M 2000 *J. Phys. Chem.* B **104** 2824
[7] Buissette V, Moreau M, Gacoin T and Boilot J 2006 *Adv. Funct. Mater.* **16** 351
[8] Beche E, Charvin P, Perarnau D, Abanades S and Flamant G 2008 *Surf. Interface Anal.* **40** 264
    Takita Y, Qing X, Takami A, Nishiguchi H and Nagaoka K 1999 *Appl. Catal.* A **176** 11
[9] Zhou Z, Shinar R, Allison A and Shinar J 2007 *Adv. Funct. Mater.* **17** 3530
[10] Tang Y, Tehan E, Tao Z and Bright F 2003 *Anal. Chem.* **75** 2407
    Lu X and Winnik M 2001 *Chem. Mater.* **13** 3449
[11] Kang M, Trofin L, Mota M and Martin C 2005 *Anal. Chem.* **77** 6243
    Lee S, Muller A, Al-Kaysi R and Bardeen C 2006 *Nano Lett.* **6** 1420